CAIM
ISSN 2038-0909
Commun. Appl. Ind. Math. 13 (1), 2022, 57–69
DOI: 10.2478/caim-2022-0005
Review Article

Virtual Element Methods for three-dimensional Hellinger-Reissner elastostatic problems

Carlo Lovadina[1,2*], Michele Visinoni[1]

[1]Dipartimento di Matematica, Università di Milano, Via Saldini 50, I-20133 Milano, Italy
[2]IMATI del CNR, Via Ferrata 1, 27100 Pavia, Italy

[*]Email address for correspondence: carlo.lovadina@unimi.it

Communicated by Giorgio Fotia
Received on 07 30, 2022. Accepted on 09 30, 2022.

Abstract

This note aims at illustrating the application of the Virtual Element Method to elasticity problems in mixed form, following the Hellinger-Reissner variational principle. In order to highlight the potential and the flexibility of our approach, we focus on a three-dimensional low-order Virtual Element scheme, but similar considerations apply to two-dimensional and higher-order methods.

Keywords: Virtual element methods; elasticity problems; hybridization procedure.

AMS subject classification: 65N30, 65N12, 65N15

1. Introduction

The Virtual Element Method (VEM) is a recent technology for the approximation of partial differential equation problems. VEM was born in 2012, see [1], as an evolution of modern mimetic schemes (see for instance [2] and the references therein), which share the same variational background of the Finite Element Method (FEM). The basic motivation of VEM is the need to construct an accurate Galerkin scheme with the following two properties.

- The flexibility to deal with highly general polygonal/polyhedral meshes, including "hanging vertexes" and non-convex shapes.
- The conformity of the method, i.e. the property to build an approximated solution which shares the same "natural" regularity as the analytical solution of the problem.

To achieve both the requirements above, the virtual element method *abandons the local polynomial approximation concept typical of FEM*, and use, instead, approximating functions which are solutions to suitable local partial differential equations (of course, connected with the original problem to solve). Therefore, in general, the discrete functions are not known pointwise, but a limited information of them are at disposal. However, the available information is sufficient for forming the stiffness matrix and the right-hand side.

In this paper we wish to present the application of VEM to the linear elastic problem in mixed form, following the so-called Hellinger-Reissner principle (see [3], for instance). More precisely, we report some of the results obtained by our research team, focusing on a three-dimensional low-order scheme. However, we remark that:

1. two-dimensional Hellinger-Reissner VEMs have been developed and analysed, both for a low-order case (see [4]) and for high-order methods (see [5]);
2. the extension to higher-order schemes for three-dimensional problems is available (see [6]).

It is interesting to notice that our approach gives rise to methods which enjoy the following basic features.

- The stress field is *a-priori* symmetric and $H(\mathbf{div})$-regular;
- all the schemes are *inf-sup* stable, see [3], and optimally convergent;
- for all the schemes we can easily perform a suitable hybridization procedure (see [7], and [8] for scalar mixed problems). Besides providing an efficient way to solve the linear system stemming from the discrete problem, this technique also allows to post-process an improved approximated displacement field.

It is well-known that, *all together*, the above properties are hardly met in the framework of the Finite Element Method, but they are within the reach of the Virtual Element Method, due to its great flexibility.

An outline of the paper is as follows. In Section 2 we introduce the equations of linear elasticity in terms of stresses and displacements. Then the Hellinger-Reissner variational formulation is presented, together with its Galerkin approximation. Afterwards, we detail the VEM discretization we are interested in, stating also the convergence result proved in [9]. Section 3 describe the hybridization technique applied to our method, as well as the error estimate for the post-processed displacement field. In Section 4 we provide a few numerical results which support and confirm the theoretical predictions. In addition, we briefly investigate on the sensitivity to the choice of the stabilization parameter involved in the numerical scheme. Finally, Section 5 draws some conclusions.

Throughout the paper, for any non-negative integer k, we denote with $\mathbb{P}_k(\omega)$ the space of polynomials of degree at most k and defined on the set $\omega \subseteq \mathbb{R}^d$ (d =1, 2, or 3). Moreover, we will use standard notations for Sobolev spaces and their norms and semi-norms.

2. The Hellinger-Reissner elasticity problem and its VEM discretization

We consider the following well-known 3D linear elasticity problem. Given a polyhedral domain $\Omega \subseteq \mathbb{R}^3$ and an external load $\mathbf{f} : \Omega \to \mathbb{R}^3$, find the symmetric stress tensor field $\boldsymbol{\sigma} : \Omega \to \mathbb{R}^{3\times 3}$ and the displacement field $\mathbf{u} : \Omega \to \mathbb{R}^3$ such that:

$$
\begin{cases} -\,\mathbf{div}\,\boldsymbol{\sigma} = \mathbf{f} & \text{in } \Omega \\ \boldsymbol{\sigma} = \mathbb{C}\boldsymbol{\varepsilon}(\mathbf{u}) & \text{in } \Omega \\ \mathbf{u} = \mathbf{0} & \text{on } \partial\Omega \end{cases} . \tag{1}
$$

For sake of simplicity, we here consider homogeneous Dirichlet boundary conditions, but other cases can be considered and treated in standard ways. Moreover, we assume that the elasticity fourth-order symmetric tensor $\mathbb{C}$ is uniformly-bounded, positive-definite and sufficiently smooth. The Hellinger-Reissner variational formulation of Problem (1) (see [3,10] for more details) is:

$$
\begin{cases} \text{Find } (\boldsymbol{\sigma}, \mathbf{u}) \in \Sigma \times U \text{ such that} \\ a(\boldsymbol{\sigma}, \boldsymbol{\tau}) + b(\boldsymbol{\tau}, \mathbf{u}) = \mathbf{0} & \forall \boldsymbol{\tau} \in \Sigma \\ b(\boldsymbol{\sigma}, \mathbf{v}) = -(\mathbf{f}, \mathbf{v}) & \forall \mathbf{v} \in U \end{cases} \tag{2}
$$

where

$$
U := \left[L^2(\Omega)\right]^3, \qquad \Sigma := \{\boldsymbol{\tau} \in H(\mathbf{div};\Omega) \ : \ \boldsymbol{\tau} \text{ symmetric}\}, \tag{3}
$$

with $H(\mathbf{div};\Omega) := \left\{\boldsymbol{\tau} \in \left[L^2(\Omega)\right]^{3\times 3} : \ \mathbf{div}\,\boldsymbol{\tau} \in \left[L^2(\Omega)\right]^3\right\}$. The spaces U and Σ are equipped with their natural norms. Furthermore, the bilinear forms in (2) are defined as:

$$
a(\boldsymbol{\sigma}, \boldsymbol{\tau}) := \int_\Omega \mathbb{C}^{-1}\boldsymbol{\sigma} : \boldsymbol{\tau} \, \mathrm{d}\Omega, \qquad b(\boldsymbol{\sigma}, \mathbf{u}) := \int_\Omega \mathbf{div}\,\boldsymbol{\sigma} \cdot \mathbf{u} \, \mathrm{d}\Omega, \tag{4}
$$

and $(\cdot,\cdot)$ denotes the usual L^2 scalar product. As it is well-known this problem is well-posed [3].

A typical Galerkin approximation of Problem (2) can be written as follows:

$$\begin{cases} \text{Find } (\boldsymbol{\sigma}_h, \mathbf{u}_h) \in \Sigma_h \times U_h \text{ such that} \\ a_h(\boldsymbol{\sigma}_h, \boldsymbol{\tau}_h) + b_h(\boldsymbol{\tau}_h, \mathbf{u}_h) = 0 & \forall \boldsymbol{\tau}_h \in \Sigma_h \\ b_h(\boldsymbol{\sigma}_h, \mathbf{v}_h) = -(\mathbf{f}, \mathbf{v}_h)_h & \forall \mathbf{v}_h \in U_h. \end{cases} \tag{5}$$

where U_h and Σ_h are the finite dimensional approximating spaces for the displacement and stress field, respectively. Moreover, $a_h(\cdot,\cdot)$, $b_h(\cdot,\cdot)$ and $(\mathbf{f},\cdot)_h$ are suitable approximations of the corresponding bilinear and linear forms. We consider a particular Galerkin scheme in the spirit of the Virtual Element Method introduced in [1]. We thus need to introduce the approximation spaces and the approximated form, as described below.

2.1. *Definition of the approximating spaces*

We first introduce a star-shaped polyhedral tessellation Ω_h of Ω, h being the mesh-size, and we define two finite dimensional spaces $U_h \subseteq U$ and $\Sigma_h \subseteq \Sigma$, tailored to the mesh Ω_h. Similarly to the finite element approach, U_h and Σ_h will be obtained by gluing suitable *local* approximation spaces. Hence, we first fix an element $E \in \Omega_h$.

For the local approximation space of the displacement field we then select:

$$U_h(E) = \left\{ \mathbf{v}_h \in \left[L^2(E)\right]^3 \ : \ \mathbf{v}_h \in \mathrm{RM}(E) \right\}, \tag{6}$$

where

$$\mathrm{RM}(E) := \left\{ \mathbf{r}(\mathbf{x}) = \boldsymbol{\alpha} + \boldsymbol{\omega} \wedge \left(\mathbf{x} - \mathbf{x}_E\right) \ \text{ s.t. } \boldsymbol{\alpha},\ \boldsymbol{\omega} \in \mathbb{R}^3 \right\} \tag{7}$$

is the space of the local infinitesimal rigid body motions. Accordingly, for $U_h(E)$ the following degrees of freedom can be taken:

$$\mathbf{v}_h \longrightarrow \int_E \mathbf{v}_h \cdot \mathbf{r} \; \mathrm{d}E \qquad \forall\, \mathbf{r} \in \mathrm{RM}(E). \tag{8}$$

It follows that $\dim(U_h(E)) = \dim(\mathrm{RM}(E)) = 6$. The global discrete displacement space U_h is then defined by

$$U_h = \left\{ \mathbf{v}_h \in \left[L^2(\Omega)\right]^3 \ : \ \mathbf{v}_{h|E} \in U_h(E) \qquad \forall E \in \Omega_h \right\}. \tag{9}$$

We remark that this space is made by explicitly known functions, as they are piecewise polynomials.

Instead, the virtual element concept comes into play when defining the local approximation space for the stress field. In fact, we set:

$$\begin{aligned} \Sigma_h(E) := \Big\{ \boldsymbol{\tau}_h \in & H(\mathbf{div}; E) \ : \ \exists\, \mathbf{w}^* \in \left[H^1(E)\right]^3 \text{ such that } \boldsymbol{\tau}_h = \mathbb{C}\boldsymbol{\varepsilon}(\mathbf{w}^*); \\ & (\boldsymbol{\tau}_h\, \mathbf{n})_{|f} \in T_h(f) \quad \forall f \in \partial E; \quad \mathbf{div}\, \boldsymbol{\tau}_h \in \mathrm{RM}(E) \Big\}, \end{aligned} \tag{10}$$

where, for each face $f \in \partial E$:

$$T_h(f) := \left\{ \boldsymbol{\psi}(\tilde{\mathbf{x}}) = \mathbf{t}_f + a\left[\mathbf{n}_f \wedge (\mathbf{x}(\tilde{\mathbf{x}}) - \mathbf{x}_f)\right] + p_1(\tilde{\mathbf{x}})\mathbf{n}_f, \quad \text{s.t.} \quad a \in \mathbb{R},\ p_1(\tilde{\mathbf{x}}) \in \mathbb{P}_1(f) \right\}. \tag{11}$$

Here above, $\mathbf{n}_f$ is the outward normal to the face f, on which we have introduced 2D local coordinates $\tilde{\mathbf{x}}$. Moreover, $\mathbf{t}_f$ is an arbitrary vector tangent to f and $\mathbf{x}(\tilde{\mathbf{x}})$ is the three dimensional position vector of a point on f, determined by $\tilde{\mathbf{x}}$. We remark that $T_h(f)$ can be seen as the space of vector functions whose tangential component is a 2D rigid body motion defined on f, while the normal component is a linear polynomial on f. Accordingly, for the local space $\Sigma_h(E)$ the following degrees of freedom can be taken.

- For each face f of the element E, the three degrees of freedom which determine the tangential component of the tractions:

$$\tau_h \longrightarrow \int_f (\tau_h\,\mathbf{n})_{|f} \cdot \Big[\boldsymbol{\theta}_f + \alpha\big[\mathbf{n}_f \wedge (\mathbf{x}(\tilde{\mathbf{x}}) - \mathbf{x}_f)\big]\Big]\ \mathrm{d}f. \tag{12}$$

  Above, $\alpha \in \mathbb{R}$ and $\boldsymbol{\theta}_f$ is an arbitrary vector tangent to the face f.
- For each face f of the element E, the three degrees of freedom which determine the normal component of the tractions:

$$\tau_h \longrightarrow \int_f (\tau_h\,\mathbf{n})_{|f} \cdot \Big[q_1(\tilde{\mathbf{x}})\mathbf{n}_f\Big]\ \mathrm{d}f \qquad \forall\, q_1(\tilde{\mathbf{x}}) \in \mathbb{P}_1(f). \tag{13}$$

It is easy to see that, for every $\tau_h \in \Sigma_h(E)$, the divergence $\mathbf{div}\,\tau_h$ is completely determined by the boundary information (degrees of freedom) at our disposal, see Proposition 3.1 in [9] for more details. In addition, this set of degrees of freedom is unisolvent for the space $\Sigma_h(E)$, so that its dimension is

$$\dim(\Sigma_h(E)) = 6\, n_f^E,$$

where n_f^E is the number of element faces. Furthermore, we notice that these degrees of freedom are entirely defined on each polyhedron face, contrary to what happens to the Finite Element approach, where nodal degrees of freedom must be always present, see [11,12] for instance. This nice property is crucial for the simple hybridization procedure detailed in Section 3. The global discrete stress space Σ_h is then defined by

$$\Sigma_h := \Big\{\tau_h \in H(\mathbf{div};\Omega)\ :\ \tau_{h|E} \in \Sigma_h(E) \qquad \forall E \in \Omega_h\Big\}. \tag{14}$$

We remark that the regularity condition $\tau_h \in H(\mathbf{div};\Omega)$ essentially requires that the tractions $\tau_h\mathbf{n}$ are continuous across each face of the mesh Ω_h.

2.2. *Definition of discrete bilinear forms*

Given an element $E \in \Omega_h$ we notice that for every $\tau_h \in \Sigma_h(E)$ and $\mathbf{v}_h \in U_h(E)$ the local mixed term

$$b_E(\boldsymbol{\sigma}_h, \mathbf{v}_h) = \int_E \mathbf{div}\,\boldsymbol{\sigma}_h \cdot \mathbf{v}_h\ \mathrm{d}E \tag{15}$$

is computable by means of the information at our disposal: the stress and displacement degrees of freedom. Analogously, since $\mathbf{v}_h \in \mathrm{RM}(E)$ the right-hand side term

$$(\mathbf{f}, \mathbf{v}_h) = \int_\Omega \mathbf{f}\,\mathbf{v}_h\ \mathrm{d}\Omega = \sum_{E\in\Omega_h} \int_E \mathbf{f}\,\mathbf{v}_h\ \mathrm{d}E \tag{16}$$

is computable via quadrature rules for polyhedral domain. Therefore, there is not need to introduce any approximation of the global terms $b(\cdot,\cdot)$ and $(\mathbf{f},\cdot)$. Hence, it holds (cf. (5)):

$$b_h(\boldsymbol{\sigma}_h, \mathbf{v}_h) := \sum_{E\in\Omega_h} b_E(\boldsymbol{\sigma}_{h|E}, \mathbf{v}_{h|E}) = b(\boldsymbol{\sigma}_h, \mathbf{v}_h)$$

and

$$(\mathbf{f}, \mathbf{v}_h)_h = (\mathbf{f}, \mathbf{v}_h).$$

Instead, to compute the local bilinear form

$$a_E(\boldsymbol{\sigma}_h, \tau_h) = \int_E \mathbb{C}^{-1}\boldsymbol{\sigma}_h : \tau_h\ \mathrm{d}E \tag{17}$$

we need to use the standard VEM technique [1,13], since we do not explicitly know the discrete stresses in the element E. We introduce a suitable projection operator onto local polynomial functions, which is computable via the degrees of freedom. In our case, we introduce $\Pi_E : \Sigma_h(E) \to [\mathbb{P}_0(E)]_s^{3\times 3}$, by requiring

$$\int_E \Pi_E \boldsymbol{\tau}_h : \boldsymbol{\pi}_0 = \int_E \boldsymbol{\tau}_h : \boldsymbol{\pi}_0 \, \mathrm{d}E \qquad \forall \boldsymbol{\pi}_0 \in [\mathbb{P}_0(E)]_s^{3\times 3}. \tag{18}$$

This projection operator is computable. Indeed, we notice that each $\boldsymbol{\pi}_0 \in [\mathbb{P}_0(E)]_s^{3\times 3}$ can be written as the symmetric gradient of a linear vectorial function, i.e. $\boldsymbol{\pi}_0 = \boldsymbol{\varepsilon}(\mathbf{p}_1)$, with $\mathbf{p}_1 \in [\mathbb{P}_1(E)]^3$. Hence, using the divergence theorem, the right-hand side of (18) becomes

$$\int_E \boldsymbol{\tau}_h : \boldsymbol{\pi}_0 \, \mathrm{d}E = \int_E \boldsymbol{\tau}_h : \boldsymbol{\varepsilon}(\mathbf{p}_1) \, \mathrm{d}E = -\int_E \mathbf{div}\, \boldsymbol{\tau}_h \cdot \mathbf{p}_1 \, \mathrm{d}E + \int_{\partial E} (\boldsymbol{\tau}_h \mathbf{n}) \cdot \mathbf{p}_1 \, \mathrm{d}f$$

which is clearly computable through the degrees of freedom in $\Sigma_h(E)$. Then, the approximation of $a_E(\cdot,\cdot)$ reads:

$$\begin{aligned} a_E^h(\boldsymbol{\sigma}_h, \boldsymbol{\tau}_h) &:= a_E(\Pi_E \boldsymbol{\sigma}_h, \Pi_E \boldsymbol{\tau}_h) + s_E\left((I - \Pi_E)\boldsymbol{\sigma}_h, (I - \Pi_E)\boldsymbol{\tau}_h\right) \\ &= \int_E \mathbb{C}^{-1}(\Pi_E \boldsymbol{\sigma}_h) : (\Pi_E \boldsymbol{\tau}_h) \, \mathrm{d}E + s_E\left((I - \Pi_E)\boldsymbol{\sigma}_h, (I - \Pi_E)\boldsymbol{\tau}_h\right), \end{aligned} \tag{19}$$

where $s_E(\cdot,\cdot)$ is a suitable stabilization term which scales like the continuous bilinear form $a_E(\cdot,\cdot)$. We propose the following choice:

$$s_E(\boldsymbol{\sigma}_h, \boldsymbol{\tau}_h) := \kappa_E \, h_E \int_{\partial E} (\boldsymbol{\sigma}_h \mathbf{n}) \cdot \boldsymbol{\tau}_h \mathbf{n} \, \mathrm{d}f. \tag{20}$$

Above, κ_E is a positive constant to be chosen according to $\mathbb{C}^{-1}$, while h_E is the diameter of the element E. The global approximated bilinear form $a_h(\cdot,\cdot)$ to be used in Problem (5) is then defined as

$$a_h(\boldsymbol{\sigma}_h, \boldsymbol{\tau}_h) := \sum_{E \in \Omega_h} a_E^h(\boldsymbol{\sigma}_{h|E}, \boldsymbol{\tau}_{h|E}).$$

With all the quantities defined in Sections 2.1 and 2.2, we are ready to build the discrete problem (5). In [9] we have proved that the method is *inf-sup* stable, see [3], for instance. Moreover, under the usual regular assumptions on the mesh and on the solution to Problem (2), for the discrete Problem (5) we have the following error estimate

$$||\boldsymbol{\sigma} - \boldsymbol{\sigma}_h||_\Sigma + ||\mathbf{u} - \mathbf{u}_h||_U \le Ch, \tag{21}$$

where C is independent of h. Finally, for homogeneous and isotropic materials, the above estimate is robust with respect to the value of the bulk modulus, thus the scheme is optimally convergent also in the nearly incompressible regime.

3. Hybridization procedure

The hybridization procedure in the framework of mixed methods is a computational technique to re-write the discrete problem in a different way. Its main feature is that the resulting linear system is symmetric and positive definite, instead of the original indefinite one, cf. [7]. Moreover, by this procedure it is possible to get a better approximation of the displacement solution, see [8].

More precisely, in our case the hybridization technique and its consequences can be split into the following three steps, which will be detailed below:

- the introduction of suitable Lagrange multipliers to impose the stress $H(\mathbf{div})$-conformity;
- the application of the static condensation algorithm to reduce computational costs;
- the design of a suitable post-processing procedure.

3.1. *Imposing $H(\mathbf{div})$-conformity via Lagrange multipliers*

This first step is characterized by the introduction of Lagrange multipliers to impose the required continuity constraints across the interfaces, rather than enforcing them directly in the approximation space. To accomplish this goal in a simple manner, it is crucial that the boundary stress degrees of freedom are defined only on the faces and not on the element vertices. The idea is the following: instead of considering the standard stress VEM space

$$\Sigma_h := \left\{ \boldsymbol{\tau}_h \in H(\mathbf{div}, \Omega) \ : \ \boldsymbol{\tau}_{h|E} \in \Sigma_h(E) \quad \forall E \in \mathcal{T}_h \right\}, \tag{22}$$

we introduce the larger discrete space

$$\tilde{\Sigma}_h := \left\{ \boldsymbol{\tau}_h \in \left[L^2(\Omega)\right]^{2\times 2} \ : \ \boldsymbol{\tau}_{h|E} \in \Sigma_h(E) \quad \forall E \in \mathcal{T}_h \right\}. \tag{23}$$

Now, calling $\mathcal{F}_h^I$ the set of the internal faces of Ω_h, we define the space of Lagrange multipliers by (cf. (11)):

$$\Lambda_h(\mathcal{F}_h^I) := \left\{ \boldsymbol{\mu}_h \in \left[L^2(\mathcal{F}_h^I)\right]^3 : \ \boldsymbol{\mu}_{h|f} \in T_h(f) \quad \forall\, f \in \mathcal{F}_h^I \right\}. \tag{24}$$

where, with a little abuse of notation, we denote with $L^2(\mathcal{F}_h^I)$ the L^2 space defined on the interior skeleton of Ω_h, i.e., the union of $f \in \mathcal{F}_h^I$. Notice that the Lagrange multipliers are defined only on the *internal* faces $\mathcal{F}_h^I$ because their role is to match the normal component of the stresses, as required by the $H(\mathbf{div}, \Omega)$ regularity. To force such a continuity, we introduce the discrete bilinear form

$$c_h(\cdot,\cdot) : \tilde{\Sigma}_h(\Omega_h) \times \Lambda_h(\mathcal{F}_h^I) \to \mathbb{R} \tag{25}$$

defined as:

$$c_h(\boldsymbol{\tau}_h, \boldsymbol{\mu}_h) := -\sum_{E\in\Omega_h} \int_{\partial E^I} \boldsymbol{\mu}_h \cdot \boldsymbol{\tau}_h\, \mathbf{n}\; \mathrm{d}f \quad \forall \boldsymbol{\tau}_h \in \tilde{\Sigma}_h(\Omega_h),\ \forall \boldsymbol{\mu}_h \in \Lambda_h(\mathcal{F}_h^I), \tag{26}$$

where $\partial E^I = \partial E \cap \mathcal{F}_h^I$. We observe that although $\boldsymbol{\tau}_h$ is virtual, such bilinear form is computable. Indeed, we are integrating over faces where both $\boldsymbol{\mu}_h$ and $\boldsymbol{\tau}_h\mathbf{n}$ are polynomials. Then, the hybridized version of Problem (5) reads as follows:

$$\begin{cases} \text{Find } (\boldsymbol{\sigma}_h, \mathbf{u}_h, \boldsymbol{\lambda}_h) \in \tilde{\Sigma}_h \times U_h \times \Lambda_h(\mathcal{F}_h^I) \text{ such that} \\ a_h(\boldsymbol{\sigma}_h, \boldsymbol{\tau}_h) + b(\boldsymbol{\tau}_h, \mathbf{u}_h) + c_h(\boldsymbol{\tau}_h, \boldsymbol{\lambda}_h) = 0 & \forall \boldsymbol{\tau}_h \in \tilde{\Sigma}_h, \\ b(\boldsymbol{\sigma}_h, \mathbf{v}_h) = -(\mathbf{f}, \mathbf{v}_h) & \forall \mathbf{v}_h \in U_h, \\ c_h(\boldsymbol{\sigma}_h, \boldsymbol{\mu}_h) = 0 & \forall \boldsymbol{\mu}_h \in \Lambda_h(\mathcal{F}_h^I). \end{cases} \tag{27}$$

It can be proven, see [14], that Problem (27) is well-posed; more importantly, if $(\boldsymbol{\sigma}_h, \mathbf{u}_h, \boldsymbol{\lambda}_h) \in \tilde{\Sigma}_h \times U_h \times \Lambda_h(\mathcal{F}_h^I)$ solves problem (27), then $(\boldsymbol{\sigma}_h, \mathbf{u}_h)$ is also the solution of Problem (5).

3.2. *Static condensation*

The second step is merely an algebraic manipulation which leads to a symmetric and positive definite linear system the can be efficiently solved. Let us start recalling the matrix form of Problem (27):

$$\begin{pmatrix} \tilde{A} & \tilde{B} & \tilde{C} \\ \tilde{B}^T & O & O \\ \tilde{C}^T & O & O \end{pmatrix} \begin{pmatrix} \boldsymbol{\sigma}_h \\ \mathbf{u}_h \\ \boldsymbol{\lambda}_h \end{pmatrix} = \begin{pmatrix} O \\ \tilde{F} \\ O \end{pmatrix}. \tag{28}$$

Here above the symbol $\sim$ highlights that the quantity under consideration refers to the (discontinuous) space (23), rather than to the conforming one (22). One of the advantages of the discontinuous stress degrees of freedom is that the matrices $\tilde{A}$ and $\tilde{B}$, corresponding to the discrete bilinear form $a_h(\cdot,\cdot)$ and the mixed term $b(\cdot,\cdot)$ are block matrices. Each block corresponds to a single element, so that Gauss elimination of $\boldsymbol{\sigma}_h$ and $\mathbf{u}_h$ from system (28) can be permformed elementwise, see [14] for details. Thus, we end up with the following linear system involving only the multipliers:

$$H\boldsymbol{\lambda}_h = R \tag{29}$$

where

$$H = \tilde{C}^T\tilde{A}^{-1}\tilde{C} - (\tilde{C}^T\tilde{A}^{-1}\tilde{B})(\tilde{B}^T\tilde{A}^{-1}\tilde{B})^{-1}(\tilde{B}^T\tilde{A}^{-1}\tilde{C}) \tag{30}$$

and

$$R = (C^T\tilde{A}^{-1}\tilde{B})(\tilde{B}^T\tilde{A}^{-1}\tilde{B})^{-1}\tilde{F}. \tag{31}$$

The matrix H is symmetric and positive definite, so that "ad-hoc" methods to solve (29) can be employed (for instance, Cholesky decomposition method). Once we have solved it to get $\boldsymbol{\lambda}_h$, the displacements and the stresses can be obtained explicitly via matrix-vector multiplication, again see [14] for details.

3.3. *Post-processing procedure*

This last step is characterized by the possibility to reconstruct a better approximation of the displacement field through a post-processing procedure. Indeed, since the Lagrange multipliers $\boldsymbol{\lambda}_h$ have the physical interpretation of (generalized) displacements, the idea is to use them to design a higher-order (non-conforming) approximation $\mathbf{u}_h^*$ of the displacement field. Our choice is based on a vectorial version of the non-conforming VEM scheme described in [15]. More precisely, the local virtual space is:

$$U_h^*(E) := \left\{\mathbf{v}_h^* \in \left[H^1(E)\right]^3 \,:\, \frac{\partial \mathbf{v}_h^*}{\partial \mathbf{n}} = \nabla\mathbf{v}_h^*\mathbf{n} \in [\mathbb{P}_0(f)]^3 \quad \forall f \in \partial E, \quad \Delta\mathbf{v}_h^* = \mathbf{0}\right\}. \tag{32}$$

Accordingly, for $U_h^*(E)$ we can take the following degrees of freedom:

$$\mathbf{v}_h^* \to \frac{1}{|f|}\int_f \mathbf{v}_h^* \,\mathrm{d}f = \Pi_0^\partial\boldsymbol{\lambda}_h, \tag{33}$$

where

$$\Pi_0^\partial : \left[L^2(\mathcal{F}_h^I)\right]^3 \to \left[\mathbb{P}_0(\mathcal{F}_h^I)\right]^2 \subseteq \Lambda_h(\mathcal{F}_h^I), \tag{34}$$

is the L^2-projection onto the space of vector constant functions. Moreover, under the usual regular assumptions on the mesh and on the solution, the following error estimates can be established, see Theorem 5.3 in [14]:

$$||\mathbf{u} - \mathbf{u}_h^*||_0 \le Ch^2. \tag{35}$$

and, if the family of meshes $\{\Omega_h\}_h$ is also quasi-uniform, it holds

$$|\mathbf{u} - \mathbf{u}_h^*|_{1,\Omega_h} = \sqrt{\sum_{E\in\Omega_h} ||\nabla(\mathbf{u} - \mathbf{u}_h^*)||_{0,E}^2} \le Ch. \tag{36}$$

As usual, in the above estimates the quantity C is independent of h (and of the bulk modulus when homogeneous and isotropic materials are considered).

4. Numerical results

In this section, we validate the theoretical results by means of numerical experiments on a problem for which the analytical solution is explicitly known; then we briefly present a computational investigation on the sensitivity of the method solution to the stabilization parameter κ_E, see (20).

Test Case. Given the unit cube $\Omega = [0,1]^3$, we consider a 3D elastic problem with the following analytical displacement solution $\mathbf{u} = (u_1, u_2, u_3)^T$:

$$
\begin{cases} u_1 = \left(x - x^2\right) \left(y - y^2\right) (2\,z - 1) - \left(x - x^2\right) \left(z - z^2\right) (2\,y - 1) \\ u_2 = \left(y - y^2\right) \left(z - z^2\right) (2\,x - 1) - \left(x - x^2\right) \left(y - y^2\right) (2\,z - 1) \\ u_3 = \left(x - x^2\right) \left(z - z^2\right) (2\,y - 1) - \left(y - y^2\right) \left(z - z^2\right) (2\,x - 1) \end{cases} \tag{37}
$$

The stress solution $\boldsymbol{\sigma}$ and the loading term $\mathbf{f}$ are computed accordingly. For this problem we consider a homogeneous and isotropic material with Lamé coefficients $\lambda = 10^5$, $\mu = 0.5$, which corresponds to a nearly incompressible case.

We consider the four families of meshes depicted in Figure 1: standard structured cubes, Delaunay tetrahedralization of Ω, Voronoi tessellation with Lloyd algorithm to regularize the elements, Voronoi tessellation with random control points. Moreover, the parameter involved in the stabilization term (20) is always chosen as $\kappa = \kappa_E = \frac{1}{2}\mathrm{tr}(\mathbb{C}^{-1})$ for every element E (except for Section 4.4).

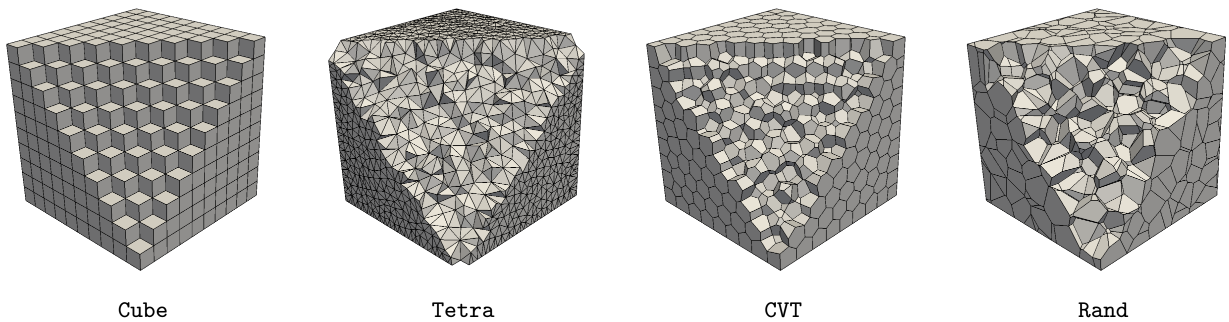

Figure 1. Overview of adopted meshes for numerical tests.

4.1. *Convergence results*

To study to convergence in actual computations, we use the following error norms:

- L^2 error norm for the displacement field: $E_{\mathbf{u}} := ||\mathbf{u} - \mathbf{u}_h||_0$.
- L^2 error on the divergence: $E_{\boldsymbol{\sigma},\mathbf{div}} := ||\,\mathbf{div}\,\boldsymbol{\sigma} - \mathbf{div}\,\boldsymbol{\sigma}_h||_0$.
- L^2 error on the projection: $E_{\boldsymbol{\sigma},\Pi} := ||\boldsymbol{\sigma} - \Pi\boldsymbol{\sigma}_h||_0$, where Π is such that $\Pi_{|E} = \Pi_E$.
- Discrete error norms for the stress field:

$$
E_{\boldsymbol{\sigma}} := \left(\sum_{f \in \mathcal{F}_h} h_f \int_f \kappa\, |(\boldsymbol{\sigma} - \boldsymbol{\sigma}_h)\mathbf{n}|^2 \right)^{1/2},
$$

where h_f is the diameter of the face f.

In Figure 2 we display the h-convergence graphs of the proposed VEM approach. As expected the method leads to an asymptotic convergence rate equal to 1 for all error norms and meshes. Moreover, the convergence graphs are close to each others, confirming the robustness of the proposed scheme with respect to element shape.

4.2. *Post-processing results*

We now show the accuracy of the post-processed displacement field obtained by the hybridization procedure. We measure the error by means of the following quantities:

$$
E^0_{\mathbf{u}_h^*} := ||\mathbf{u} - \Pi^\nabla \mathbf{u}_h^*||_0 \quad \text{and} \qquad E^1_{\mathbf{u}_h^*} := |\mathbf{u} - \Pi^\nabla \mathbf{u}_h^*|_{1,\mathcal{T}_h},
$$

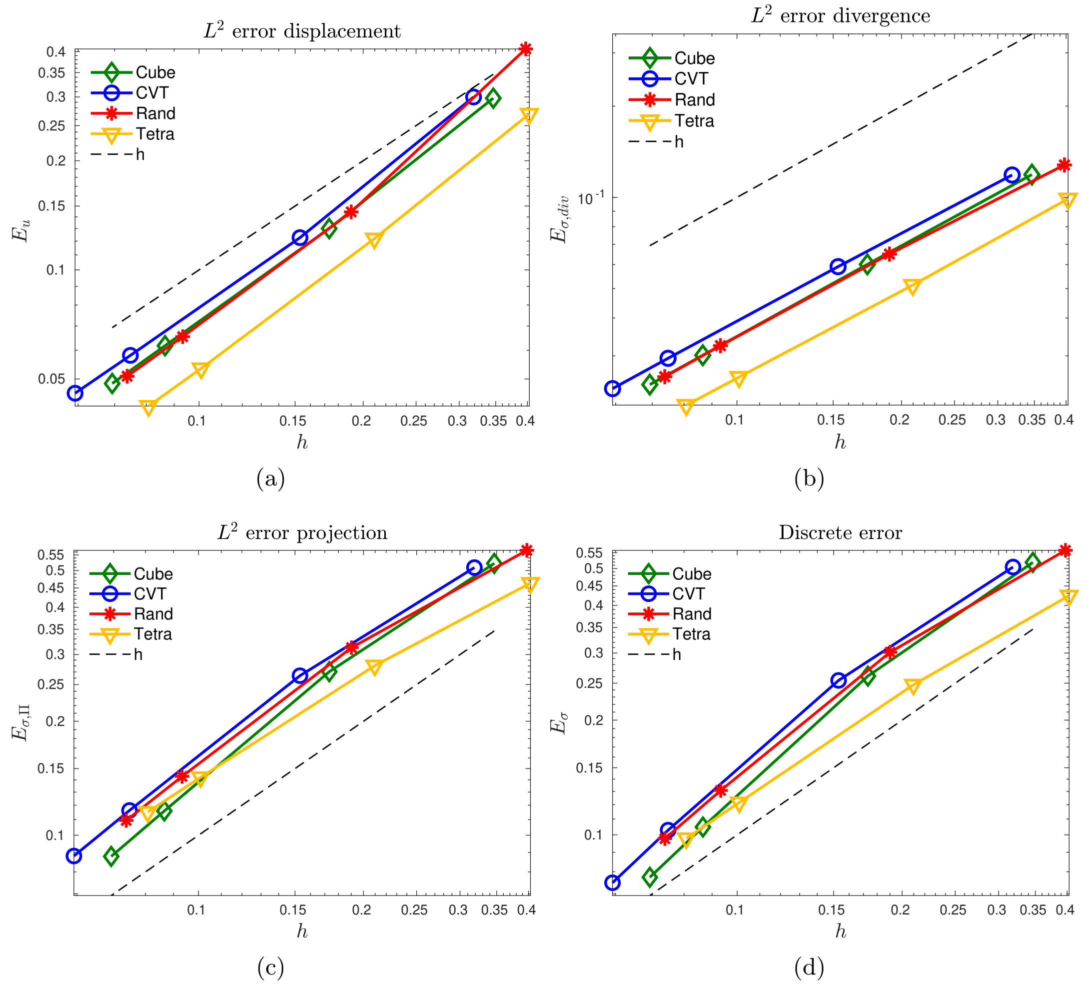

Figure 2. h-convergence results for all meshes.

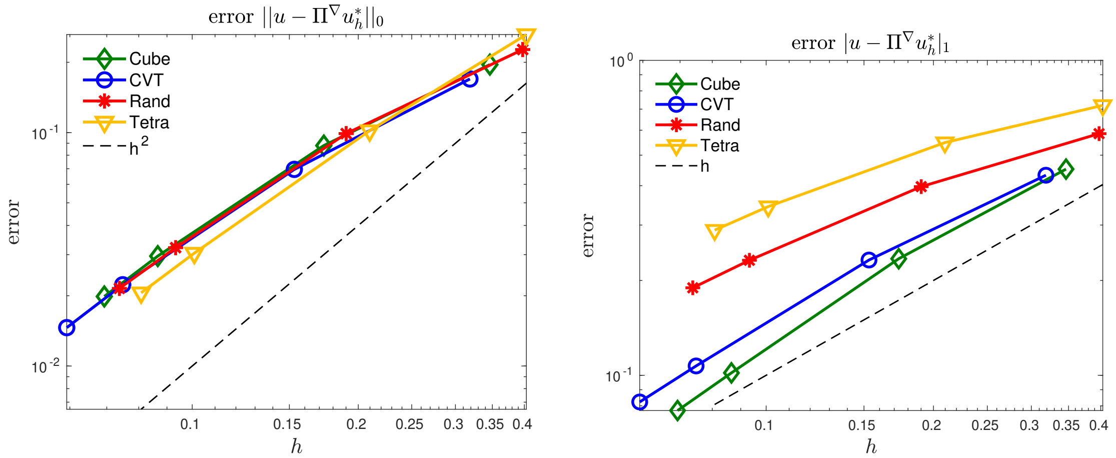

Figure 3. Post-processing. Convergence plots for the error $E^0_{\mathbf{u}_h^*}$ and $E^1_{\mathbf{u}_h^*}$ for test case 3D.

where $\mathbf{u}$ is the analytical solution, $\mathbf{u}_h^*$ represents the non-conforming reconstruction of the displacement solution and Π^∇ is the standard projection operator defined in [14,15].

Figure 3 displays the corresponding convergence histories. The convergence rate for the error $E^0_{\mathbf{u}_h^*}$ is approximately 2, while for the error $E^1_{\mathbf{u}_h^*}$ is 1, as expected by estimates (35) and (36). Although estimate (36) has been proved only for quasi-uniform meshes, the numerical tests suggest that the same behaviour occurs for more general situations (e.g., `Rand` meshes are not quasi-uniform but still a first order convergence rate takes place). Moreover, the convergence lines of each mesh are close to each others, showing, once again, the VEM robustness with respect to the mesh distortion.

4.3. *Comparison of solving time*

We show the effect of the hybridization technique on the solution time of the resulting linear system. Accordingly, we qualitatively compare the solving times between the standard low-order VEM approach (i.e. to compute the solution to the linear system stemming from Problem (5)) and the hybridized scheme procedure (i.e. to compute the solution of linear system (29) and then get $\boldsymbol{\sigma}_h$ and $\mathbf{u}_h$). We use the open-source library PETSc [16]. In particular, we use the direct solver MUMPS: LU factorization for the standard method; Cholesky for the hybridized one. Moreover, we run our test only on one processor in order to have the same setting for both the cases.

Table 1. Comparison of solving time (in seconds) between standard approach and hybridization technique for our test case

	Cube			Tetra		
Step	Standard	Hybrid		Standard	Hybrid	
1	0.09	0.13	(28.27%)	0.10	0.15	(20.57%)
2	2.93	2.23	(68.89%)	2.55	2.53	(50.94%)
3	403.44	94.19	(92.57%)	485.59	234.48	(95.34%)
4	4058.78	659.77	(97.60%)	2633.88	1283.38	(98.24%)
	CVT			Rand		
Step	Standard	Hybrid		Standard	Hybrid	
1	0.56	0.58	(44.67%)	0.75	0.76	(49.29%)
2	59.35	29.53	(88.07%)	114.25	41.37	(88.62%)
3	15778.60	3997.49	(99.10%)	22003.10	8517.07	(99.40%)
4	101685.00	26988.20	(99.73%)	147205.00	49210.70	(99.77%)

Table 1 summarizes the outcomes for each mesh refinement step. Moreover, in the column "Hybrid", we also show the percentage of time used to solve the linear system (29) (the remaining time is used for the static condensation and for computing $\boldsymbol{\sigma}_h$ and $\mathbf{u}_h$). We notice that refining the meshes, the hybridization procedure shows better performance (in time) than the standard procedure. Furthermore, we observe that this improvement becomes more and more effective as the time for solving system (29) becomes dominant (this occurs for larger and larger systems).

4.4. *Investigation on sensitivity of stabilization parameter*

To explore the sensitivity on the choice of the stabilization parameter, we consider the following test. We fix a single mesh for each type: for `Cube`, `CVT` and `Rand` families we select a mesh with 1000 elements, while for `Tetra` family we take 2449 elements (this choice corresponds to the second step of the sequences used in the previous tests). We then pick different values of the stabilization parameter, cf. (20), to show the effect of the stabilization term on the discrete solution of Problem (5). More precisely, we take κ as follows:

$$\kappa = \kappa(\alpha) = \frac{1}{2}\mathrm{tr}(\mathbb{C}^{-1})\alpha, \qquad \text{where}\, \alpha \in \left\{10^{-4}, 10^{-3}, 10^{-2}, 10^{-1}, 1, 10, 10^2, 10^3, 10^4\right\}. \tag{38}$$

In Figure 4 we plot the the errors $E_{\mathbf{u}}$, $E_{\boldsymbol{\sigma},\mathbf{div}}$, $E_{\boldsymbol{\sigma},\Pi}$ and $E_{\boldsymbol{\sigma}}$ versus the parameter α in a log-log scale. On the one hand, we notice that the best performances are reached (approximately) for $\alpha \in [10^{-1}, 1]$, which confirms that our initial choice $\kappa = \frac{1}{2}\mathrm{tr}(\mathbb{C}^{-1})$ is sensible. On the other hand, things goes wrong if we take κ "too large" or "too small". In the first case (for instance, consider $\alpha = 10^4$) the stabilization

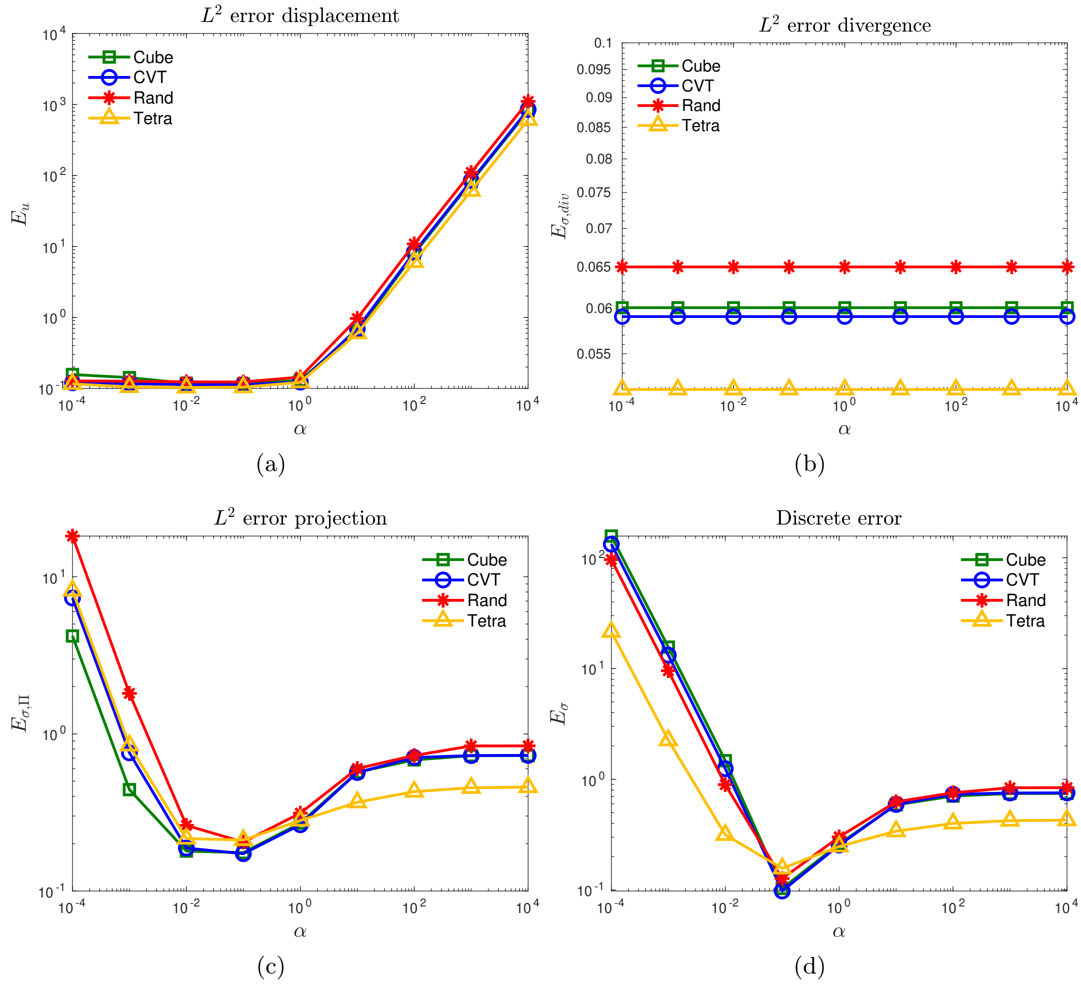

Figure 4. Investigation of stabilization parameter.

term matters much more than the consistency term in (19). From Figure 4, we notice that the error $E_{\mathbf{u}}$ grows, while the errors $E_{\boldsymbol{\sigma},\Pi}$ and $E_{\boldsymbol{\sigma}}$ are basically the same. This outcome might be interpreted by inspecting the first equation of Problem (5): if κ is "large", the bilinear form $b_h(\cdot,\cdot)$, and thus the discrete displacement $\mathbf{u}_h$, risks to be negligible. Instead, in the second case (for instance, consider $\alpha = 10^{-4}$), the stabilization term becomes "small" and the bilinear form $a_h(\cdot,\cdot)$ of Problem (5) tends to get singular: as a consequence, the discrete stresses are out of control and the corresponding errors grow (except $E_{\boldsymbol{\sigma},\mathbf{div}}$). Different considerations apply to the latter error measure $E_{\boldsymbol{\sigma},\mathbf{div}}$: from the second equation of (5) we find that it always holds

$$\mathbf{div}\,\boldsymbol{\sigma}_h = -P_h\mathbf{f},$$

where P_h denotes the L^2- projection onto U_h. Since the term $-P_h\mathbf{f}$ is of course independent of κ, the quantity $E_{\boldsymbol{\sigma},\mathbf{div}}$ is so, as well.

5. Conclusions

We have reported on some of our results concerning the Virtual Element Method applied to the Hellinger-Reissner formulation of linear elasticity problems. More precisely, we have considered a 3D low-order scheme, for which we present the relevant theoretical results, as well as some numerical outcomes. Thus, we have shown that the VEM approach is surely a valid alternative to other more classical paradigms (FEMs, for instance).

We finally remark that other many contributions about the VEM discretization of linear elasticity problems are available in the literature; for instance, we cite [17]. But one may also exploit schemes designed for the Stokes equations, see for example [18], or [19], where methods based on discrete exact sequences (e.g., see [20], [21] [22]) are considered.

Acknowledgements

The authors are members of the INdAM Research group GNCS and they were partially supported by INdAM-GNCS and the Italian MIUR (Ministero dell'Istruzione, Ministero dell'Università e della Ricerca) through the PRIN2017 Project: Virtual Element Methods: Analysis and Applications.

References

1. L. Beirão da Veiga, F. Brezzi, A. Cangiani, G. Manzini, L. D. Marini, and A. Russo, Basic principles of Virtual Element Methods, *Mathematical Models and Methods in Applied Sciences*, vol. 23, pp. 119–214, 2013.
2. L. Beirão da Veiga, K. Lipnikov, and G. Manzini, *The mimetic finite difference method for elliptic problems*, vol. 11 of *Modeling, Simulation and Applications*. Springer, 2014.
3. D. Boffi, F. Brezzi, and M. Fortin, *Mixed finite element methods and applications*, vol. 44 of *Springer Series in Computational Mathematics*. Springer, Heidelberg, 2013.
4. E. Artioli, S. de Miranda, C. Lovadina, and L. Patruno, A stress/displacement virtual element method for plane elasticity problems, *Comp. Methods Appl. Mech. Engrg.*, vol. 325, pp. 155–174, 2017.
5. E. Artioli, S. de Miranda, C. Lovadina, and L. Patruno, A family of virtual element methods for plane elasticity problems based on the hellinger-reissner principle, *Comp. Methods Appl. Mech. Engrg.*, vol. 340, pp. 978–999, 2018.
6. M. Visinoni, A family of three-dimensional virtual elements for hellinger-reissner elasticity problems, *in preparation*.
7. B. F. De Veubeke and O. C. Zienkiewicz, Displacement and equilibrium models in the finite element method, *International Journal for Numerical Methods in Engineering*, vol. 52, no. 3, pp. 287–342, 2001.
8. D. N. Arnold and F. Brezzi, Mixed and nonconforming finite element methods: implementation, postprocessing and error estimates, *ESAIM: Mathematical Modelling and Numerical Analysis*, vol. 19, pp. 7–32, 1985.
9. F. Dassi, C. Lovadina, and M. Visinoni, A three-dimensional Hellinger-Reissner virtual element method for linear elasticity problems, *Computer Methods in Applied Mechanics and Engineering*, vol. 364, p. 112910, 2020.
10. D. Braess, *Finite elements. Theory, fast solvers, and applications in elasticity theory.* Cambridge University Press, third ed., 2007.
11. D. N. Arnold and R. Winther, Mixed finite elements for elasticity, *Numerische Mathematik*, vol. 92, pp. 401–419, 2002.
12. D. N. Arnold, G. Awanou, and R. Winther, Finite elements for symmetric tensors in three dimensions, *Mathematics of Computation*, vol. 77, pp. 1229–1251, 2008.
13. L. Beirão da Veiga, F. Brezzi, L. D. Marini, and A. Russo, The hitchhiker's guide to the virtual element method, *Mathematical Models and Methods in Applied Sciences*, vol. 24, no. 8, pp. 1541–1573, 2014.
14. F. Dassi, C. Lovadina, and M. Visinoni, Hybridization of the virtual element method for linear elasticity problems, *Mathematical Models and Methods in Applied Sciences*, vol. 31, no. 14, pp. 2979–3008, 2021.
15. B. Ayuso, K. Lipnikov, and G. Manzini, The nonconforming virtual element method, *ESAIM: Mathematical Modelling and Numerical Analysis*, vol. 50, no. 3, pp. 879–904, 2016.
16. S. Balay, S. Abhyankar, M. F. Adams, J. Brown, P. Brune, K. Buschelmanm, L. Dalcin, A. Dener, V. Eijkhout, W. D. Gropp, D. Karpeyev, D. Kaushik, M. G. Knepley, D. A. May, L. C. McInnes, R. T. Mills, T. Munson, K. Rupp, P. Sanan, B. F. Smith, S. Zampini, H. Zhang, and H. Zhang, PETSc Web page. https://www.mcs.anl.gov/petsc, 2019.

17. L. Beirão da Veiga, F. Brezzi, and L. D. Marini, Virtual Elements for linear elasticity problems, *SIAM J. Numer. Anal.*, vol. 51, pp. 794–812, 2013.
18. L. Beirão da Veiga, C. Lovadina, and G. Vacca, Divergence free virtual elements for the Stokes problem on polygonal meshes, *ESAIM: Mathematical Modelling and Numerical Analysis*, vol. 51, no. 2, pp. 509–535, 2017.
19. L. Beirão da Veiga, D. Mora, and G. Vacca, The Stokes complex for virtual elements with application to Navier-Stokes flows, *Journal of Scientific Computing*, vol. 81, no. 2, pp. 990–1018, 2019.
20. D. Arnold, *Finite Element Exterior Calculus*, vol. 93 of *CBMS-NSF Regional Conference Series in Applied Mathematics*. SIAM, Philadelphia, 2018.
21. D. Arnold, D. Boffi, and F. Bonizzoni, Finite element differential forms on curvilinear cubic meshes and their approximation properties, *Numerische Mathematik*, vol. 129, no. 1, pp. 1–20, 2015.
22. F. Bonizzoni and G. Kanschat, H^1-conforming finite element cochain complexes and commuting quasi-interpolation operators on cartesian meshes, *Calcolo*, vol. 58, no. 18, 2021.